Inorganic Chemistry
Article

Inorg. Chem. **2010**, *49*, 977–988 **977**
DOI: 10.1021/ic9017745

Family of V(III)-Tristhiolato Complexes Relevant to Functional Models of Vanadium Nitrogenase: Synthesis and Electronic Structure Investigations by Means of High-Frequency and -Field Electron Paramagnetic Resonance Coupled to Quantum Chemical Computations.

Shengfa Ye,[†] Frank Neese,*[,†] Andrew Ozarowski,[‡] Dmitry Smirnov,[‡] J. Krzystek,*[,‡] Joshua Telser,*[,§] Ju-Hsiou Liao,[∥] Chen-Hsiung Hung,[⊥] Wei-Chen Chu,[#] Yi-Feng Tsai,[#] Rong-Chin Wang,[#] Kun-Yuan Chen,[#] and Hua-Fen Hsu*[,#]

[†]*Institut für Physikalische und Theoretische Chemie, Universität Bonn, D-53115 Bonn, Germany,* [‡]*National High Magnetic Field Laboratory, Florida State University, Tallahassee, Florida 32310,* [§]*Department of Biological, Chemical and Physical Sciences, Roosevelt University, Chicago, Illinois 60605,* [∥]*Department of Chemistry, National Chung Cheng University, Chia-Yi 621, Taiwan,* [⊥]*Institute of Chemistry, Academia Sinica, Taipei 115, Taiwan, and* [#]*Department of Chemistry, National Cheng Kung University, Tainan 701, Taiwan*

Received September 8, 2009

A series of V(III) complexes of varying coordination number (5, 6, and 7) all containing the PS3 ligand (PS3 = trianion of tris(2-thiophenyl)phosphine and its derivatives with other phenyl substituents) has been prepared and structurally characterized. The complexes have general formula $[V(PS3)L_n]^{0,-}$, where $n = 1$ (from L = Cl^-, 1-Me-Im, N_3^-), 2 (from L = 2,2′-bpy; counting each N of the bidentate ligand), and 3 (from L = 1-Me-Im, N_2H_4). The complexes have also been investigated by direct current (DC) magnetic susceptibility and high-frequency and -field electron paramagnetic resonance (HFEPR). HFEPR, supported by magnetometry, has provided accurate spin Hamiltonian parameters that describe the $S = 1$ spin ground state of the complexes. Of particular interest are the zero-field splitting (zfs) parameters which, together with structural data, are the empirical starting point for detailed computational studies. The computational methods included density functional theory (DFT), which was only marginally successful, and more advanced ab initio methods (CASSCF and SORCI). The zfs in these complexes is relatively small in magnitude ($|D| \approx 1\ cm^{-1}$) and is the result of multiple, often counteracting, spin−orbit coupling (SOC) and spin−spin coupling (SSC) contributions. The specific origin of each of these contributions is described in detail. The results indicate the level of electronic structure calculation possible for transition metal complexes even with multiple unpaired electrons and highly covalent, heavier atom donor ligands.

Introduction

The increasing interest in the study of vanadium chemistry stems from the important roles of this element in biological systems, as well as from its medical applications.[1−5] In particular, the finding of a vanadium containing nitrogenase has motivated us and others to investigate vanadium complexes with thiolate ligands, mimicking the sulfido environment of the vanadium site in the enzyme.[6] To date, we have explored the reactions of V(III) ion with trisbenzenethiolatophosphine ligands,[7] generically abbreviated as PS3.[8,9] Because of the flexibility of geometries adopted by the V(III) ion, those reactions led to a collection of 5-, 6-, and 7-coordinate V(III) compounds, $[V(PS3)L_n]^{0,-}$ ($n = 1-3$), by binding to a PS3 ligand and other small molecules/ions (L = Cl^-, N_3^-, Im, 1-Me-Im, 2−2′-bpy, N_2H_4; Scheme 1). It is worth noting that compound **1** can carry out the catalytic reduction of N_2H_4 to ammonia, serving as a functional model of vanadium nitrogenase.[9]

*To whom correspondence should be addressed. E-mail: neese@thch.uni-bonn.de (F.N.), krzystek@magnet.fsu.edu (J.K.), jtelser@roosevelt.edu (J.T.), konopka@mail.ncku.edu.tw (H.H.).

(1) Rehder, D. *Bioinorganic Vanadium Chemistry*; John Wiley & Sons: New York, 2008.
(2) Crans, D. C.; Smee, J. J.; Gaidamauskas, E.; Yang, L. *Chem. Rev.* **2004**, *104*, 849–902.
(3) Baran, E. J. *J. Braz. Chem. Soc.* **2003**, *14*, 878–888.
(4) Guest editor: Hirao, T. *Coord. Chem. Rev.* **2003**, *237*, 1−286. (A special issue containing contributions from 3rd International Symposium on Chemistry and Biological Chemistry of Vanadium).
(5) Guest editors: Rehder, D. Conte, V. *J. Inorg. Biochem.* **2000**, *80*, 1−194. (A special issue containing contributions from 2nd International Symposium on Chemistry and Biological Chemistry of Vanadium).
(6) Janas, Z.; Sobota, P. *Coord. Chem. Rev.* **2005**, *249*, 2144–2155.
(7) Block, E.; Ofori-Okai, G.; Zubieta, J. *J. Am. Chem. Soc.* **1989**, *111*, 2327–2329.
(8) Hsu, H.-F.; Chu, W.-C.; Hung, C.-H.; Liao, J.-H. *Inorg. Chem.* **2003**, *42*, 7369–7371.
(9) Chu, W.-C.; Wu, C.-C.; Hsu, H.-F. *Inorg. Chem.* **2006**, *45*, 3164–3166.

Published on Web 12/22/2009

Scheme 1

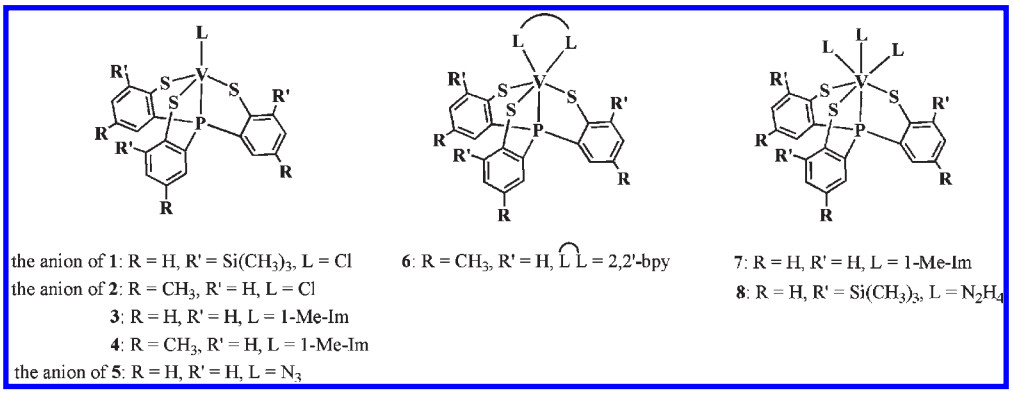

To further study these complexes in depth, a full understanding of their electronic structures is essential. In contrast to the V(IV) ion, with its $3d^1$ electronic configuration and $S = 1/2$ spin ground state, which can be studied by conventional (e.g., X-band, ~9 GHz) electron paramagnetic resonance (EPR),[10,11] the V(III) ion, $3d^2$, is a non-Kramers system and usually EPR-silent because of its integer-spin ground state, $S = 1$. However, by utilizing high-frequency and -field EPR (HFEPR) the zero-field splitting (zfs) and ground state g values of V(III) ion can be precisely measured.[12−15] The observation of V(III) in the blood cells of sea squirts[2,16] has initiated some research focusing on V(III) complexes with aminocarboxylate ligands,[17−19] including spectroscopic studies involving HFEPR.[20] In contrast, spectroscopic investigations on V(III) complexes with S-donor ligands are very rare. Thus, in this work, we investigate the electronic structures of complexes **1**−**8** by applying several physical methods including HFEPR spectroscopy, variable-temperature and variable field magnetometry.

To understand the origin of the zfs in transition metal complexes, it is necessary to resort to electronic structure approaches. Unfortunately, the first-principle theory of zfs is still in its infancy and only recently have systematic studies appeared in the literature that predict zfs of transition metal complexes using density functional theory (DFT) or correlated ab initio methods (recently reviewed elsewhere[21]). The accuracy with which zfs can be predicted appears to vary greatly among different d^N configurations. Hence, it is necessary to gain as much experience in this area as possible. In this respect the present work on d^2 systems not only is of specific interest in enhancing our understanding of V(III) complexes but also is a necessary step in the application of theoretical methods to derive zfs of transition metal ions in general.

Experimental Section

Materials and Syntheses. All procedures were carried out under argon or dinitrogen with standard Schlenk or glovebox techniques. The PS3 ligand system,[7] $VCl_3(THF)_3$,[22] and compounds **1**, **2**,[9] **3**, and **8**[8] were synthesized according to literature procedures. The syntheses of compounds **4**, **6**, and **7** are described in the Supporting Information. The preparation of compound **5** will be addressed elsewhere. Solvents were dried according to standard procedures. Otherwise all starting materials were obtained commercially and used without further purification.

Crystallographic Structure Determination. The X-ray crystallographic structures of **1**, **2**, **3**, and **8** have been reported previously.[8,9] The structures of complexes **4**, **6**, and **7** were determined in this work, and their crystallographic parameters are listed in Table S1 (Supporting Information). Each crystal was sealed in a capillary with epoxy resin. Diffraction measurements were carried out on a Bruker SMART 1000 CCD diffractometer with graphite-monochromated Mo Kα radiation ($\lambda = 0.7107$ Å). Least-squares refinement of the positional and anisotropic thermal parameters for the contribution of all nonhydrogen atoms and fixed hydrogen atoms was based on F^2. A SADABS absorption correction was made.[23] The SHELXTL structural refinement program was employed.[24] All nonhydrogen atoms except those of the methanol solvent molecules in $\mathbf{6}\cdot 2CH_3OH$ were refined with anisotropic displacement factors. The positions of all of the hydrogen atoms were calculated by using the riding model.

Magnetic Measurements and Analysis. Powder samples of complexes **1**, **3**, **5**−**8** were studied by variable temperature (2−300 K) direct current (DC) magnetic susceptibility measurements, in most cases at multiple applied magnetic fields (0.5−55 kOe). Samples were placed in gel cap sample holders and immobilized in *n*-eicosane. The measurements were performed on a Quantum Design MPMS-7 SQUID magnetometer.

(10) Chasteen, N. D. In *Biological Magnetic Resonance*; Berliner, L. J., Reuben, J., Eds.; Plenum: New York, 1981; Vol. 3, p 53−119.
(11) Smith, T. S., II; LoBrutto, R.; Pecoraro, V. L. *Coord. Chem. Rev.* **2002**, *228*, 1–18.
(12) Krzystek, J.; Fiedler, A. T.; Sokol, J. J.; Ozarowski, A.; Zvyagin, S. A.; Brunold, T. C.; Long, J. R.; Brunel, L.-C.; Telser, J. *Inorg. Chem.* **2004**, *43*, 5645–5658.
(13) Beaulac, R.; Tregenna-Piggott, P. L. W.; Barra, A.-L.; Weihe, H.; Luneau, D.; Reber, C. *Inorg. Chem.* **2006**, *45*, 3399–3407.
(14) Krzystek, J.; Ozarowski, A.; Telser, J. *Coord. Chem. Rev.* **2006**, *250*, 2308–2324.
(15) Tregenna-Piggott, P. L. W.; Spichiger, D.; Carver, G.; Frey, B.; Meier, R.; Weihe, H.; Cowan, J. A.; McIntyre, G. J.; Zahn, G.; Barra, A.-L. *Inorg. Chem.* **2004**, *43*, 8049–8060.
(16) Michibata, H.; Yamaguchi, N.; Uyama, T.; Ueki, T. *Coord. Chem. Rev.* **2003**, *237*, 41–51.
(17) Alonso, P. J.; Forniés, J.; García-Monforte, M. A.; Martín, A.; Menjón, B. *Chem. Commun.* **2001**, 2138–2139.
(18) Meier, R.; Boddin, M.; Mitzenheim, S.; Schmid, V.; Schönherr, T. *J. Inorg. Biochem.* **1998**, *69*, 249–252.
(19) Schönherr, T.; Schmid, V.; Meier, R. *Spectrochim. Acta, Part A* **1998**, *54*, 1659–1669.
(20) Telser, J.; Wu, C.-C.; Chen, K.-Y.; Hsu, H.-F.; Smirnov, D.; Ozarowski, A.; Krzystek, J. *J. Inorg. Biochem.* **2009**, *103*, 487–495.
(21) Neese, F. Zero-field splitting in *Calculation of NMR and EPR parameters. Theory and Applications*; Kaupp, M., Bühl, M., Malkin, V. G., Eds.; Wiley-VCH: Weinheim, Germany, 2004.
(22) Manzer, L. E. *Inorg. Synth.* **1982**, *21*, 138.
(23) Sheldrick, G. M. *SADABS*; University of Göttingen: Göttingen, Germany, 1996.
(24) Sheldrick, G. M. *SHELXTL*; Siemens Analytical X-ray Instruments Inc.: Madison, WI, 1994.

Corrections were made for the diamagnetic susceptibility of the complexes using Pascal's constants.[25]

High-Frequency and -Field EPR. Spectra were recorded using primarily the EMR Facility at the NHMFL, with some experiments performed at the Millimeter and Submillimeter Wave Facility. The former facility uses fixed-frequency solid-state sources ranging from 24 to 600 GHz, and a superconducting 15/17 T magnet. The latter employs tunable-frequency backward wave oscillators operating in the 150−700 GHz range and the resistive "Keck" magnet, enabling 0−25 T field sweeps. Detection was provided with an InSb hot electron bolometer (QMC Ltd., Cardiff, U.K.). For detection purposes the magnetic field was modulated at 1−40 kHz frequency. A Stanford Research Systems SR830 lock-in amplifier converted the modulated signal to DC voltage. Samples were cooled to cryogenic temperatures using an Oxford Instruments continuous-flow cryostat and controller.

Analysis of Magnetic and HFEPR Data. The variable-temperature magnetic susceptibility data and the multifrequency HFEPR data were each fitted using the same spin Hamiltonian for $S = 1$ systems composed of Zeeman and zfs terms:[26]

$$\mathscr{H} = \beta B \bullet g \bullet S + D(S_z^2 - S(S+1)/3) + E(S_x^2 - S_y^2) \qquad (1)$$

Fits of the magnetic data used the locally written program DSUSFITP,[27] which calculates a powder pattern average of the molecular magnetization using the above spin Hamiltonian. The procedure involved simultaneous best fits, using a nonlinear least-squares methodology, to variable-temperature susceptibility data collected at several magnetic fields.

Field-swept HFEPR on polycrystalline solids provides turning points in powder-pattern spectra. Their frequency dependencies were recorded as two-dimensional data sets (see below), and spin Hamiltonian parameters were then fitted to these data by use of a non-linear least-squares procedure based on the well-known formulas resulting from the exact solution of the equations for triplet states of arbitrary orientation.[28] Further details of the tunable-frequency EPR methodology are given elsewhere.[29]

Computational Details. It has been demonstrated that computed zfs parameters are extremely sensitive to small structural changes.[30] For this reason calculations of the **D** tensor for each model, $V(PS_3^H)(NH_3)$ (**4′**), $V(PS_3^H)(NH_3)_2$ (**6′**), and $V(PS_3^H)(NH_3)_3$ (**7′**) were carried out on each of two structures: (*i*) a completely optimized geometry and (*ii*) a constrained model wherein the V−N, V−P, and V−S bond distances were fixed at the experimental distances of the parent systems (respectively, **4**, **6**, and **7**). All calculations in this work were carried out with the ORCA program package.[31] All geometry optimizations were done with the BP86[32−34] density functional. The TZVP[21,35] (for V, N, P, and S atoms), and SV(P) (for other atoms) basis sets[35] were applied in combination with the TZV/J (V, N, P, and S atoms) and SV/J (remaining) auxiliary basis sets.[36,37] The RI approximation[36−38] was used to accelerate the calculations.

The zfs (**D** tensor) consists of two contributions: the direct electron−electron spin−spin coupling (SSC), which is present to first order in perturbation theory, and the spin−orbit coupling (SOC), which is present to second order in perturbation theory.[39,40] The SSC contribution (D^{SSC}) is usually believed to dominate the zfs of organic radicals,[41] while the second-order SOC contribution has invariably been claimed to provide the dominant contribution to the zfs of transition metal complexes.[42] However, it has recently been shown that SOC does not always strongly dominate and that the SSC term must be included to arrive at quantitative results.[30,43]

In a sum-over-states formulation, the SOC contribution to the **D** tensor contains three terms that arise from excited states of the same total spin as the ground state as well as those differing by one unit of spin-angular momentum, explicitly[44]

$$D_{kl} = D_{kl}^{SSC} + D_{kl}^{SOC-(0)} + D_{kl}^{SOC-(-1)} + D_{kl}^{SOC-(+1)} \qquad (2)$$

with

$$D_{kl}^{SOC-(0)} = -\frac{1}{S^2} \sum_{b(S_b=S)} \Delta_b^{-1} \langle 0SS| \sum_i h_i^{k,SOC} s_{i,0} |bSS\rangle \langle bSS| \sum_i h_i^{l,SOC} s_{i,0} |0SS\rangle$$

$$D_{kl}^{SOC-(-1)} = -\frac{1}{S(2S-1)} \sum_{b(S_b=S-1)} \Delta_b^{-1} \langle 0SS| \sum_i h_i^{k,SOC} s_{i,+1} |bS-1S-1\rangle \langle bS-1S-1| \sum_i h_i^{l,SOC} s_{i,-1} |0SS\rangle \qquad (3)$$

$$D_{kl}^{SOC-(+1)} = -\frac{1}{(S+1)(2S+1)} \sum_{b(S_b=S+1)} \Delta_b^{-1} \langle 0SS| \sum_i h_i^{k,SOC} s_{i,-1} |bS+1S+1\rangle \langle bS+1S+1| \sum_i h_i^{l,SOC} s_{i,+1} |0SS\rangle$$

Here, S is the total spin of the ground state and the sums indexed by b refer to the electronically excited states $|bSS\rangle$ of the appropriate total spin. Although these equations are correct to second order in perturbation theory, they cannot be evaluated rigorously in practice because it is impossible to calculate an infinite number of excited states. Operationally, it has been found that, in agreement with ligand field theory, if one includes all appropriate multiplets within the d^N configuration under investigation one often obtains results with acceptable accuracy.[45,46] Alternatively, every sum-over-states equation can

(25) Boudreaux, E. A.; Mulay, L. N. *Theory and Application of Molecular Paramagnetism*; J. Wiley & Sons: New York, 1976.
(26) Abragam, A.; Bleaney, B. *Electron Paramagnetic Resonance of Transition Ions*; Dover Publications, Inc.: New York, 1986.
(27) Reisner, E.; Telser, J.; Lippard, S. J. *Inorg. Chem.* **2007**, *46*, 10754–10770.
(28) Baranowski, J.; Cukiepda, T.; Jezowska-Trzebiatowska, B.; Kozlowski, H. *Chem. Phys. Lett.* **1976**, *39*, 606–608.
(29) Krzystek, J.; Zvyagin, S. A.; Ozarowski, A.; Trofimenko, S.; Telser, J. *J. Magn. Reson.* **2006**, *178*, 174–183.
(30) Zein, S.; Duboc, C.; Lubitz, W.; Neese, F. *Inorg. Chem.* **2008**, *47*, 134–142.
(31) Neese, F. *ORCA* − an ab initio, Density Functional and Semiempirical Program Package Version 2.6 2008 ed.; Universität Bonn: Bonn, Germany, 2007.
(32) Becke, A. D. *Phys. Rev. A* **1988**, *38*, 3098–3100.
(33) Perdew, J. P. *Phys. Rev. B* **1986**, *34*, 7406.
(34) Perdew, J. P. *Phys. Rev. B* **1986**, *33*, 8822–8824.
(35) Schäfer, A.; Huber, C.; Ahlrichs, R. *J. Chem. Phys.* **1994**, *100*, 5829–5835.
(36) Eichkorn, K.; Weigend, F.; Treutler, O.; Ahlrichs, R. *Theor. Chim. Acta* **1997**, *97*, 119–124.
(37) Eichkorn, K.; Treutler, O.; Öhm, H.; Häser, M.; Ahlrichs, R. *Chem. Phys. Lett.* **1995**, *240*, 283–289.
(38) Eichkorn, K.; Treutler, O.; Öhm, H.; Häser, M.; Ahlrichs, R. *Chem. Phys. Lett.* **1995**, *242*, 652–660.
(39) Harriman, J. E. *Theoretical Foundation of Electron Spin Resonance*; Academic Press: New York, 1978.
(40) McWeeny, R. *Methods of Molecular Quantum Mechanics*; Academic Press: London, 1992.
(41) Schweiger, A.; Jeschke, G. *Principles of Pulse Electron Paramagnetic Resonance*; Oxford University Press: Oxford, U.K., 2001.
(42) Griffith, J. S. *The Theory of Transition Metal Ions*; Cambridge University Press: Cambridge, 1964.
(43) Neese, F. *J. Am. Chem. Soc.* **2006**, *128*, 10213–10222.
(44) Neese, F.; Solomon, E. I. *Inorg. Chem.* **1998**, *37*, 6568–6582.
(45) Pierloot, K. In *Computational photochemistry*; Olivucci, M., Ed.; Elsevier: Amsterdam, 2005; Vol. 16, p 279−315.
(46) Bolvin, H. *ChemPhysChem* **2006**, *7*, 1575–1589.

be exactly translated into a linear-response equation.[47,48] Unlike the sum-over-states formulations, the analytic derivatives that enter the linear response equations can be rigorously evaluated for any given approximate electronic structure methods. The linear response theory of the **D** tensor has only recently been developed and explained in detail elsewhere.[49]

The SSC contributions are calculated from the equation of McWeeny and Mizuno,[50]

$$D_{kl}^{SSC} = \frac{g_e^2 \quad \alpha^2}{4\,S(2S-1)} \sum_{\mu\nu} \sum_{\kappa\tau} \{P_{\mu\nu}^{\alpha-\beta} P_{\kappa\tau}^{\alpha-\beta} - P_{\mu\kappa}^{\alpha-\beta} P_{\nu\tau}^{\alpha-\beta}\} \langle \mu\nu | r_{12}^{-5} \{3 r_{12,k} r_{12,l} - \delta_{kl} r_{12}\} \kappa\tau \rangle \quad (4)$$

in which the spin density matrix $\mathbf{P}^{\alpha-\beta}$ was obtained on the basis of the spin-unrestricted natural orbital (UNO) determinant.[51]

The DFT calculations of the zfs of the model complexes in the present study were performed with the BP86 density functional using the TZV(2d,2p) basis set for all atoms.[35]

Complete active space self-consistent field (CASSCF) calculations were also carried out to complement the DFT results. The CASSCF calculations are based on quasi-degenerate perturbation theory (QDPT) that amounts to simultaneously diagonalizing the Born−Oppenheimer and SOC operators in the basis of the state-averaged CASSCF (SA-CASSCF) roots describing the triplet- and singlet multiplets arising from the d^2 configuration.[52] Thus, the active space was chosen to consist of two electrons in the five V 3d-based molecular orbitals (CAS(2,5)); again the TZV(2d,2p) basis set[35] was employed for all elements. In the CASSCF calculations, the orbitals were determined by the average of 10 triplet and 15 singlet roots. Subsequent diagonalization of the SOC matrix in terms of the preselected roots of the spin-free Hamiltonian yields the energies for low lying spin−orbit split components of the electronic ground and d-d excited states. Thus, this treatment may be thought of as an ab initio realization of a complete ligand-field theory that also takes care of differential orbital covalency. Of course, CASSCF is not a highly accurate method if metal−ligand bonds become considerably covalent. However, for the complexes studied in this work it is expected to perform fairly well. Similar to the DFT treatment, the application of the McWeeny and Mizuno equation[50] to multiconfigurational wave functions was used to estimate the SSC contribution.

For selected cases we have performed more rigorous multireference configuration interaction (MRCI) calculations in form of the spectroscopy oriented configuration interaction (SORCI[53]) on top of the CASSCF reference space. To reduce the computational cost, the seven coordinate complex **7′** was approximated by $V(PH_3)(SH)_3(NH_3)_3$ (**7″**). In the SORCI calculations, the thresholds T_{pre}, T_{nat}, and T_{sel} were set to 10^{-5}, 10^{-5}, and 10^{-6} Eh, respectively.

Results

A. Synthesis. The syntheses of complexes **1**−**3** and **8** have been reported previously.[8,9] Complexes **4** and **5**[54] were also obtained by a procedure very similar to that for isolating **3**; in these cases by adding excess 1-Me-Im and N_3^-, respectively, to the mixture of $VCl_3(THF)_3$ and PS3 ligands. Instead of adding a unidentate ligand, addition of the bidentate ligand, 2,2′- bpy, to the reaction mixture of $VCl_3(THF)_3$ and PS3′ gave a six-coordinate compound, [V(PS3′)(2,2′-bpy)] (**6**). A crystalline solid of complex **7**, $[V(PS3^H)(1\text{-Me-Im})_3]$, was precipitated from the reaction of $[V(PS3^H)(1\text{-Me-Im})]$ [8] with excess 1-Me-Im in THF at −20 °C. However, complex **7** in solution was not stable at room temperature because of the dissociation of bound 1-Me-Im molecules.

B. X-ray Crystallography. Complexes **1**−**8** have all been structurally characterized by X-ray crystallography, and **1**− **3** and **8** have been described previously.[8,9] Oak Ridge Thermal Ellipsoid Plot (ORTEP) diagrams of **4**, **6**, and **7** are presented in Figure 1. The structures of **1**−**5**, with generic formula $[V(PS3)L]^{0,-}$, are very similar and all adopt distorted trigonal bipyramidal geometries with the variable ligand (L = Cl^-, Im, 1-Me-Im, N_3^-) *trans* to the apical P atom of the PS3 system.[8,9] The structure of complex **6** consists of a distorted octahedral geometry, where vanadium binds to a quadridentate PS3′ ligand and a bidentate bpy molecule. The overall geometry around vanadium ion in the seven-coordinate complexes, **7** and **8**, is best described as a capped octahedron in which the three S donor atoms of PS3 and three unidentate ligands form two triangular faces of the octahedron.[8] The average V−S bond distances are dramatically different and in an increasing order for five-, six-, and seven-coordinated compounds. They are in the range of 2.31−2.32 Å, 2.39 Å, and 2.50−2.54 Å, respectively, in agreement with V−S bond distances of reported V(III) thiolate complexes (Supporting Information, Table S2).[55−63] The average P−V−S angle of these complexes varies with different geometries (82−84° for **1**−**5**, 79° for **6**, and 72−74° for **7** and **8**), reflecting the flexibility of PS3 ligand system.

C. Magnetic Measurements. Powder samples of complexes **1**, **3**, **5**−**8** were studied by variable temperature (2−300 K) DC magnetic susceptibility measurements, in most cases at multiple applied magnetic fields (0.5−55 kOe). All of the complexes exhibited qualitatively the same magnetic susceptibility behavior at low temperature, showing a sharp drop in μ_{eff} (χT) at $T < \sim 30$ K from maximal values of $\mu_{eff} \approx 2.4-2.8$. This range is within that expected for the spin-only value for a spin triplet (μ_{eff} = 2.83 for g = 2.00); the observed slightly lower values are fully expected because SOC in the less-than-half-filled V(III) ion yields $g < 2.0$. The low temperature drop in μ_{eff}

(47) Gauss, J. In *Modern Methods and Algorithms in Quantum Chemistry*; Grotendorst, J., Ed.; John von Neumann Institute for Computing: Jülich, Germany, 2000; Vol. NIC series Vol. 3, p 1.
(48) Helgaker, T.; Jørgensen, P.; Handy, N. C. *Theor. Chim. Acta* **1989**, *76*, 227–245.
(49) Neese, F. *J. Chem. Phys.* **2007**, *127*, 164112.
(50) McWeeny, R.; Mizuno, Y. *Proc. R. Soc. Lond. A* **1961**, *259*, 554–557.
(51) Sinnecker, S.; Neese, F. *J. Phys. Chem. A* **2006**, *110*, 12267–12275.
(52) Ganyushin, D.; Neese, F. *J. Chem. Phys.* **2006**, *125*, 024103.
(53) Neese, F. *J. Chem. Phys.* **2003**, *119*, 9428.
(54) Hsu, H.-F. unpublished result.
(55) Nekola, H.; Wang, D.; Grüning, C.; Gätjens, J.; Behrens, A.; Rehder, D. *Inorg. Chem.* **2002**, *41*, 2379–2384.
(56) Davies, S. C.; Hughes, D. L.; Janas, Z.; Jerzykiewicz, L. B.; Richards, R. L.; Sanders, J. R.; Silverston, J. E.; Sobota, P. *Inorg. Chem.* **2000**, *39*, 3485–3498.
(57) Randall, C. R.; Armstrong, W. H. *J. Chem. Soc., Chem. Commun* **1988**, 986.
(58) Higgs, T. C.; Ji, D.; Czernuszewicz, R. S.; Matzanke, B. F.; Schunemann, V.; Trautwein, A. X.; Helliwell, M.; Ramirez, W.; Carrano, C. J. *Inorg. Chem.* **1998**, *37*, 2383–2392.
(59) Farahbakhsh, M.; Nekola, H.; Schmidt, H.; Rehder, D. *Chem. Ber.* **1997**, *130*, 1129–1133.
(60) Tsagkalidis, W.; Rehder, D. *J. Biol. Inorg. Chem.* **1996**, *1*, 507–514.
(61) Dean, N. S.; Folting, K.; Lobkovsky, E.; Christou, G. *Angew. Chem., Int. Ed. Engl.* **1993**, *32*, 594.
(62) Szeymies, D.; Krebs, B.; Henkel, G. *Angew. Chem., Int. Ed. Engl.* **1983**, *22*, 885.
(63) Wang, D.; Behrens, A.; Farahbakhsh, M.; Gätjens, J.; Rehder, D. *Chem.—Eur. J.* **2003**, *9*, 1805–1813.

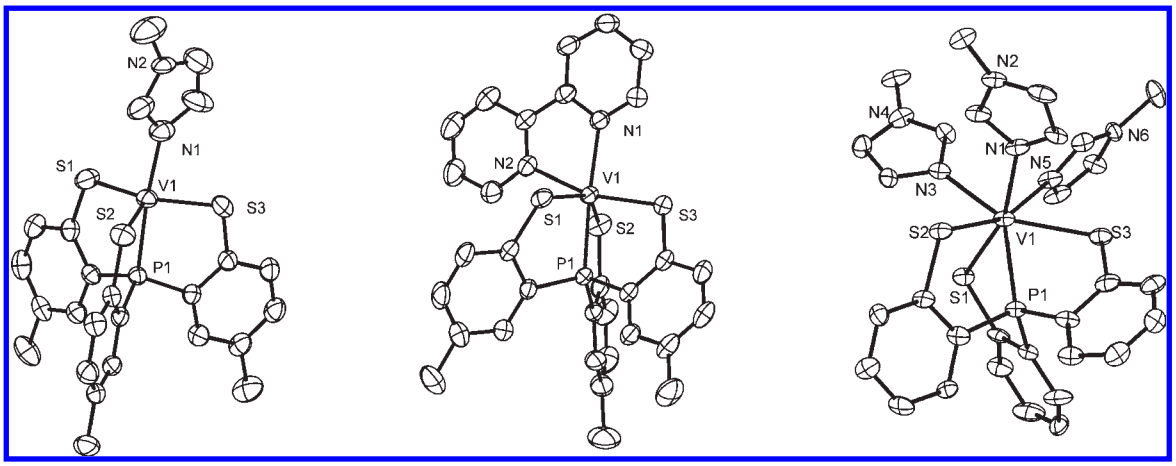

Figure 1. X-ray crystal structures of [V(PS3′)(1-Me-Im)] (**4**) (left), [V(PS3′)(2,2′-bpy)] (**6**) (middle) and [V(PS3^{H})(1-Me-Im)$_3$] (**7**) (right). Thermal ellipsoids shown at 35% probability, hydrogen atoms omitted for clarity. Selected bond distances (Å) and angles (deg): for **4**: V1—P1 2.376(1), V1—S1 2.298(2), V1—S2 2.305(2), V1—S3 2.302(2), V1—N1 2.127(4), S1—V1—P1 83.57(5), S2—V1—P1 83.44(5), S3—V1—P1 83.31(5), N1—V1—P1 175.08(14); for **6**: V1—P1 2.3803(7), V1—S1 2.4290(7), V1—S2 2.3888(8), V1—S3 2.3610(7), V1—N1 2.172(2), V1—N2 2.1670(19), S1—V1—P1 76.34(2), S2—V1—P1 80.65(2), S3—V1—P1 81.43(2), N1—V1—P1 168.85(6), N2—V1—P1 113.76(6), N1—V1—N2 74.24(8); for **7**: V1—P1 2.447(4), V1—S1 2.490(9), V1—S2 2.522(6), V1—S3 2.544(7), V1—N1 2.25(1), V1—N2 2.26(1), V1−N3 2.22(1), S1—V1—P1 72.7(1), S2—V1—P1 74.1(1), S3—V1—P1 70.5(1), N5—V1—P1 125.4(3), N1—V1—P1 125.0(3), N3—V1—P1 136.7(3), N5—V1—N1 87.6(4), N5—V1—N3 81.1(4), N1—V1—N3 85.0(4).

is a consequence of zfs,[64,65] whose value was estimated by fits of the multifield susceptibility data for each complex. The higher temperature ($T > \sim$100 K) behavior of the complexes was variable; in most cases, at higher applied fields, the value of μ_{eff} dropped, while at lower applied fields, there was often an increase in μ_{eff}. This behavior may be due to intermolecular interactions within the microcrystalline particles. Another possible source of the failure for μ_{eff} to maintain a plateau is the contribution of excited electronic states,[65] all arising from the $^3T_{1g}$ ground state in the parent octahedral symmetry, from which the complexes of interest strongly diverge. This effect was modeled in the fits by inclusion of temperature independent paramagnetism (TIP). The magnetic data are shown in Figure 2 for complexes **1**, **5**, and **7**; corresponding plots for the remaining complexes are shown in Supporting Information, Figure S1.

The availability of HFEPR allowed us to resist the temptation to overanalyze the magnetic fits and extract fit parameters of questionable validity. We thus employed a minimal version of the spin Hamiltonian in eq 1 that fits the data adequately for all complexes studied, namely, axial zfs ($E \equiv 0$) and isotropic g values ($g_x \equiv g_y \equiv g_z = g_{iso}$). In certain cases, axial g values ($g_x \equiv g_y \neq g_z$) were employed; however, this did not significantly improve the fits. Fits of the magnetic susceptibility curves did not allow discrimination between positive and negative values for the axial zfs parameter, D; the fit parameters are summarized in Table 1, which demonstrates the equivalence of the results using the two signs of D. The inability to determine the sign of zfs would severely hamper the application of detailed computational studies based on magnetometry alone. Nevertheless, magnetometry confirms the $S = 1$ ground state of these V(III) complexes and in the case of complex **8**, provides information that was not obtainable by HFEPR.

D. High-Frequency and -Field EPR. As described above, magnetometry of the [V(PS3)L$_n$] series of complexes confirms their triplet spin ground state with sizable zfs, but is less than ideal in extracting accurate values of their spin Hamiltonian parameters. To obtain quantitative information suitable for computational analysis (section E), we subjected complexes **1**, **2**, **4**−**8** to EPR experiments. With the hindsight of past EPR experiments on V(III) complexes,[12] and in view of the magnetometric results, we applied the high-frequency and -field version of the technique as described elsewhere.[14] All the investigated complexes except **8** produced spectra that could be interpreted in terms of the triplet ($S = 1$) spin ground state of the given complex. Two examples of such spectra are shown in Figure 3 together with powder-pattern simulations using the optimized spin Hamiltonian parameters, which are listed in Table 2. Additional remarks pertaining to the EPR behavior of particular complexes are the following.

Complexes **1**, **2**, **4**, and **6** showed additional resonances on top of the dominant set, suggesting the presence of a "minority" triplet spin species with spin Hamiltonian parameters slightly different from those of the "majority species". The "minority species" parameters are difficult to determine and have not been included in Table 2. This phenomenon has been observed before,[12] appears to be characteristic for a wide variety of V(III) complexes, and has been tentatively attributed to isomorphism, such as found for V(acac)$_3$.[12] In each complex under investigation there shows a detectable V(IV) impurity, yielding a high-amplitude $g \sim 1.98$ signal. Because this resonance is almost isotropic compared with the strongly anisotropic V(III) signals, its total intensity is rather small, despite the high amplitude. In the case of complex **6**, it is strong enough, however, that the V(III) resonances are partly obscured and the precision of the spin Hamiltonian parameters from them, particularly the g values, is lower than in the other cases. Finally, complex **8** is "EPR-silent" at any frequency up to 700 GHz. We speculate that this failure is due to the extensive intermolecular hydrogen bonding network that exists in **8**, as shown in Supporting Information, Figure S2. Such a network could provide

(64) Boča, R. *Coord. Chem. Rev.* **2004**, *248*, 757–815.
(65) Boča, R. *Struct. Bonding* (*Berlin*) **2006**, *117*, 1–264.

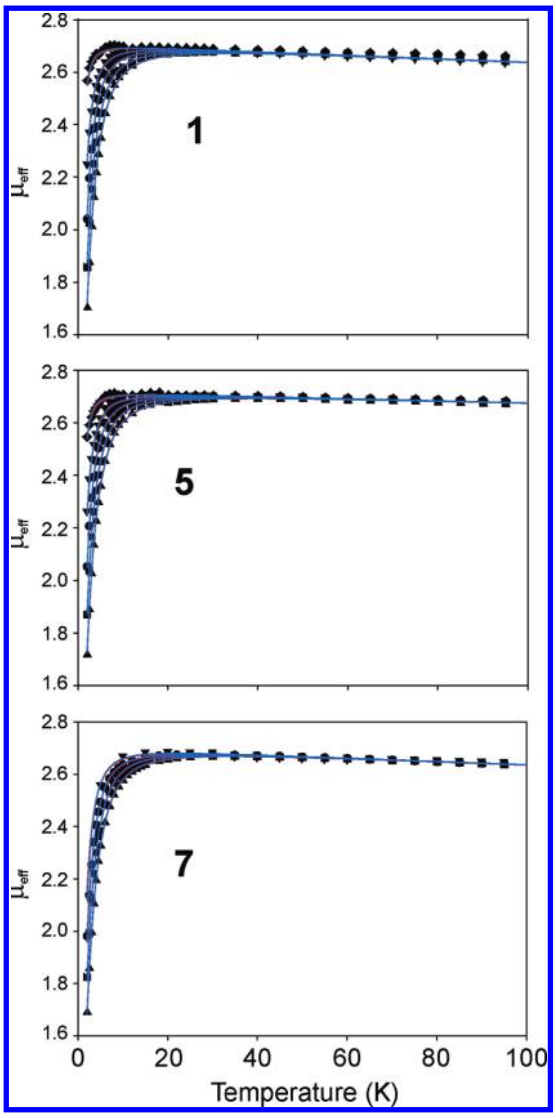

Figure 2. Plots of μ_{eff} versus temperature (2−100 K) at several applied magnetic fields for complexes **1** (top), **5** (middle), and **7** (bottom). Experimental data at each field are shown as points, using the following symbols (not all fields were used for all complexes): 10 kOe, circles; 25 kOe, upward triangles; 35 kOe, downward triangles; 45 kOe, diamonds; 55 kOe, squares. Lines indicate best fits using the parameters given in Table 1, with blue lines for $D > 0$ and red lines for $D < 0$, which lines are often totally overlapping.

efficient spin−spin relaxation pathways so that the lines are broadened beyond identification. Similar difficulties in obtaining solid state HFEPR spectra were encountered for the complex $[V(nta)(H_2O)_3]\cdot 4H_2O$, (nta is nitrilotriacetate), which also has an extensive intermolecular hydrogen-bonding network.[20] However, magnetometry is unaffected by such relaxation phenomena and provided a reasonable estimate as to the spin Hamiltonian parameters for **8** (see Table 1).

E. Computational Studies. To understand the trends in the observed zfs of the title V(III) complexes with different coordination numbers, the DFT, CASSCF, and SORCI calculations were carried out on the simplified models **4′**, **6′**, and **7′** (**7″**) as described in the Experimental Section. We will first provide the calculated D and E values before entering a detailed analysis of their physical origins.

Table 1. Spin Hamiltonian Parameters Derived from Magnetometry

complex[a]	D (cm^{-1}) [b]	g_{iso}	TIP (cm^3/mol)[c]	μ_{eff} (at 100 K) [d]
1	−1.51	1.91	-4.8×10^{-4}	2.63
	+1.28	1.91	-4.0×10^{-4}	
3	−1.26	1.83	$+7.7 \times 10^{-4}$	2.70
	+1.26	1.83	$+7.7 \times 10^{-4}$	
5	−1.80	1.92	-3.1×10^{-4}	2.66
	+1.50	1.92	-2.3×10^{-4}	
6	−6.03	1.94	$+2.6 \times 10^{-4}$	2.79
	+4.70	1.93	$+3.2 \times 10^{-4}$	
7	−3.25	1.91	-3.7×10^{-4}	2.64
	+2.86	1.91	-3.6×10^{-4}	
8	−2.71	1.95	-5.2×10^{-4}	2.68
	+2.47	1.95	-5.2×10^{-4}	

[a] Complexes **2** and **4** were not investigated by magnetometry. [b] The first set of parameters derives from fits with the constraint $D < 0$; the second with $D > 0$. [c] Inclusion of TIP led to successful fits of the high temperature region ($T > 100$ K), however, omission of TIP also adequately fit the data below ∼100 K and yielded values for D within 10% of those including TIP, and much closer for g_{iso}. [d] The μ_{eff} at 100 K is given as this typically represents roughly the maximum value; in most cases, μ_{eff} decreases above this temperature because of TIP and/or intermolecular forces. The μ_{eff} value obtained at the highest applied field (usually 55 kOe) is given. For $S = 1$, the spin-only values are in the range $2.69 \le \mu_{eff} \le 2.76$ for $g = 1.90-1.95$, which represent reasonable g_{iso} values for V(III).

Figure 3. Experimental (black traces) and simulated (red traces) powder-pattern EPR spectra of complex **5** (top part) and **7** (bottom part), recorded at 40 K and at 112 and 224 GHz, respectively. Simulation parameters as shown in Table 2. The V(IV) resonances near $g = 1.98$ in both experimental spectra were left out, and are not reproduced in the simulations.

E-1. Geometric Structure. Initially, complete geometry optimization at the BP86/TZV(P) level were performed. In comparison with the available X-ray structures, the optimized structures are in fairly good agreement with the experimental findings especially for the V−P and V−S bond distances, with deviations between theory and

Table 2. Spin Hamiltonian Parameters Derived from HFEPR Spectra at 40 K

complex[a]	D (cm^{-1})	E (cm^{-1})	g_x	g_y	g_z	ν (GHz) [b]
1	+1.08	+0.038	1.98	1.975	1.97	106
2	+1.50	0	1.97	1.97	1.97	112
4	+1.80	+0.047	1.98	1.98	1.97	222
5	+1.12	0	1.97	1.97	1.97	112
6	+1.70	+0.075	1.94	1.94	1.94	110, 219[c]
7	+0.96	+0.19	1.98	1.97	1.975	112, 224

[a] Complex **3** was not investigated by HFEPR; complex **8** was investigated by HFEPR, but did not yield observable spectra. [b] Frequenc(y/ies) employed for determination. [c] Parameters obtained at 30 K.

Table 3. ZFS Parameters (in cm^{-1}) Calculated by the DFT Method for **4′**, **6′**, and **7′**[a]

parameter	**4′**	**6′**	**7′**
D_{exp}	1.80	1.70	0.96
E_{exp}	0.047	0.075	0.19
D_{cal}	0.39 (0.37)	1.85 (0.33)	0.23 (1.22)
E_{cal}	0.01 (0.02)	0.09 (0.03)	0.07 (0.09)
D^{SOC}	−0.24 (−0.23)	−0.15 (0)	0.02 (0.35)
α→α	0.10 (0.12)	0.33 (0.45)	0 (−0.05)
$\beta\rightarrow\beta$	−0.14 (−0.11)	−0.07 (−0.07)	0 (0.01)
α→β	−0.39 (−0.42)	−0.53 (−0.45)	0.02 (0.37)
β→α	0.19 (0.18)	0.12 (0.07)	0 (0.02)
D^{SSC}	0.63 (0.61)	2.00 (0.33)	0.21 (0.87)

[a] The corresponding values for the constrained models are given in parentheses.

experiment being less than 0.02 Å (Supporting Information, Table S3). The slight overestimation of the V−N distances is readily ascribed to a difference in the donor abilities of NH_3 in the model complexes relative to imidazole and bipyridine in the actual systems.

E-2. Density Functional Theory Calculations. The zfs parameters calculated for the models on the basis of BP86 linear response equations, including their breakdown into the individual contributions, are shown in Table 3. Interestingly, DFT calculations on all of the models indicated that the dipolar SSCs provide the dominant contribution to the zfs. SSC is not considered in classical LFT treatments, such as done by some of us for other V(III) complexes,[20] indicating a potential flaw in such studies.

However, the D values calculated by DFT are in poor agreement with the experimental data for analogous compounds irrespective of whether one uses completely optimized or constrained geometries. An extremely large dependence of the results on the employed structure is clearly visible and demonstrates that zfs is a highly sensitive quantity that is very difficult to calculate accurately. Thus, for **4′** and **7′**, the calculations on the optimized structures predict D values that are too low by a factor of ∼4, while for **6′** the results are close to the measured value. By contrast, the computations on the constrained geometries significantly underestimate the D value in **4′** and **6′** by a factor of 5, while in the case of **7′** the calculations slightly overestimate the zfs. In terms of the individual contributions from SOC to the zfs, the spin-flip transitions (α→β) are the most important. However, as will be worked out in detail later, they even have the wrong sign in the case of **4′** and **6′**. This is testimony to the limitations of DFT methods in describing spin flip phenomena.[66,67] Since no systematic trend can be deduced from the DFT results, we have tried to resort to more accurate ab initio methods to calculate the zfs in the model systems.

Table 4. ZFS Parameters (in cm^{-1}) Calculated Using the Ab Initio Methods for **4′**, **6′**, **7′**, and **7″**[a]

parameter (cm^{-1})	**4′**	**6′**	**7′**	**7″**	**7″**
D_{exp}	1.80	1.70	0.96	0.96	0.96
E_{exp}	0.047	0.075	0.19	0.19	0.19
method	CASSCF	CASSCF	CASSCF	CASSCF	SORCI
D_{cal}	3.5 (2.0)	3.9 (3.4)	−1.0 (−0.5)	−0.7 (−0.4)	1.2 (1.1)
E_{cal}	0 (0)	0.8 (0.3)	0.1 (0)	0 (0)	0 (0)
D^{SOC}	2.5 (1.2)	2.5 (2.7)	−0.7 (−0.4)	−0.5 (−0.3)	−0.2 (0.1)
E^{SOC}	0 (0)	0.4 (0.3)	0.1 (0)	0 (0)	0 (0)
D^{SSC}	1.0 (0.8)	1.6 (0.7)	−0.4 (−0.1)	−0.2 (−0.1)	1.4 (1.0)
E^{SSC}	0 (0)	0.4 (0)	0 (0)	0 (0)	0 (0)

[a] The corresponding values for the constrained models are given in parentheses.

E-3. Ab Initio Calculations. Multideterminantal methods are imperative to properly describe multiplet effects and spin couplings.[68] Given the size of the model complexes in the present study, the CASSCF method is the suitable starting point. The smallest reasonable active space was chosen as two active electrons occupying the five metal d-based orbitals (CAS(2,5)). In the CASSCF calculations all 10 of the possible triplet states as well as 15 singlet states were calculated and included into the "infinite-order" SOC treatment. The data are shown in Table 4.

In the case of the model complexes **4′** and **6′**, the computed zfs-tensors are in reasonable agreement with the experimental data on similar molecules, especially for the constrained models. The SOC contributions to the zfs predicted by the CASSCF method are significantly larger than those by the DFT method (see section E-2, Table 3) such that the SOC terms are now the dominant contributions to the zfs, which is in sharp contrast to the DFT results. More importantly in **4′** and **6′** the signs of SOC contributions are reversed relative to the DFT calculations.

Surprisingly, the CASSCF method predicts the wrong sign of the total D value in **7′**. To pursue this issue, the computationally more demanding SORCI method has been employed on top of the CAS(2,5) reference state. The SORCI calculations were carried out on the simplified model $V(NH_3)_3(PH_3)(SH)_3$ (**7″**) (C_3 symmetry). Quite pleasingly, the calculated D value had excellent agreement with the experiment. Inspection of Table 4 reveals that for **7″** the SSC contribution to the zfs dominates over the SOC contribution and hence determines the final sign of the D value. By contrast, the CASSCF calculations predicted the opposite sign of the SSC contribution that results in the wrong sign in the final D value. In comparison with **4′** and **6′**, in which the SOC parts are the dominant contributions to the final D values, in **7′** or **7″** the SOC contribution is significantly reduced such that the SSC term determines the final sign of the D-value. Since the constrained models predicted

(66) Wang, F.; Ziegler, T. *J. Chem. Phys.* **2004**, *121*, 12191–12196.

(67) Vahtras, O.; Rinkevicius, Z. *J. Chem. Phys.* **2007**, *126*, 114101–114113.

(68) Neese, F. *Coord. Chem. Rev.* **2009**, *253*, 526–563.

slightly better results, the following discussion was based on these models.

E-4. Electronic Structure. To gain deeper insight into the origin of the zfs, as determined by ab initio calculations, a detailed electronic structure analysis is required. Qualitatively, the most important contribution to the zfs stems from single electron excitations within the metal d-shell and must therefore be analyzed in detail.

E-4-1. Five-Coordinate Complex 4′. As expected from ligand field theory, the trigonal bipyramidal geometry of **4′** (C_{3v} point group) leads to a $^3A_2$ ground state with d_{xz} and d_{yz} as the singly occupied molecular orbitals (SOMOs). The important single excitations within the metal d-shell are those from the degenerate 1e($d_{xz,yz}$) MOs to the unoccupied degenerate 2e($d_{x2-y2,xy}$) set. Two alternative spin couplings are possible for two unpaired electrons in four orbitals. Therefore such excitations give rise to three triplet excited states: $^3A_1$(1e→2e), $^3A_2$(1e→2e) and ^3E(1e→2e), as well as three singlet excited states: $^1A_1$(1e→2e), $^1A_2$(1e→2e) and ^1E(1e→2e), as indicated in Figure 4. A similar analysis applies to the excitation from the 1e-set to 1a_1(d_{z2}) MO which results in a triplet (^{3}E(1e→1a_1)) and a singlet excited state (^{1}E(1e→1a_1)). In addition, the spin-flip transition into the degenerate 1e-set yields two singlet states of $^1A_1$-(1e→1e) and ^{1}E(1e→1e) symmetry.

E-4-2. Six-Coordinate Complex 6′. The N2PS3 coordination sphere in **6′** is distorted octahedral with three thiolate ligands occupying the equatorial plane. They destabilize the π-antibonding d_{xy}-based MO relative to other two t_{2g} orbitals. Thus, the two SOMOs are d_{xz}- and d_{yz}-based metal d orbitals and therefore this bonding pattern leads to an orbitally nondegenerate ground state of $^3A_2$ symmetry. Consequently, the spin-Hamiltonian formalism is applicable. To employ symmetry arguments, an effective C_{4v} symmetry is used to denote the excited states. Single electron excitations from SOMOs (d_{xz} and d_{yz}) to unoccupied metal d-based MO and intra-SOMO transitions produce a range of triplet and singlet states with different symmetries ^{3,1}E(1e→1b_2), $^{3,1}A_1$(1e→1b_1), ^{3,1}E(1e→1a_1), $^1A_1$(1e→1e), $^1B_1$(1e→1e) and $^1A_1$(1e→1e) as indicated in Figure 5.

E-4-3. Seven-Coordinate Complex 7′. In **7′**, the metal ion is coordinated in a capped octahedral arrangement (C_3 point group) with three S donor atoms of the PS3 ligand and three NH_3 (hydrazine in **7**) groups forming two triangular faces of the octahedron. The ground state of **7′** is ^{3}A because of single occupation of the degenerate 1e($d_{x^2-y^2,xy}$) orbitals. However, one can identify in its SOMOs significant contributions from the other d-based e-set (e($d_{xz,yz}$)), which may be due to the fairly large out-of-plane distortion of the V center relative to the plane defined by the three S atoms (0.645 Å for **7′** vs 0.216 Å for **4′**). Promoting one electron from the 1e-set to the unoccupied metal d-based MOs gives rise to a series of triplet and singlet states of different symmetries ^{3,1}E(1e→1a_1), ^{3,1}aA-(1e→2e), ^{3,1}bA(1e→2e), and ^{3,1}E(1e→2e), as indicated in Figure 6. Two additional singlet excited states ^{1}A(1e→2e) and ^{1}E(1e→2e) arise from intra-1e spin-flip transitions.

E-5. Ligand Field Analysis. The computations indicate that there are major contributions from singlet and triplet excited states to the **D** tensor. By reference to eq 2, we can make semi-quantitative estimates of the contributions of the leading excited states to the zfs parameters. The wave functions used in the treatments are summarized in the Supporting Information.

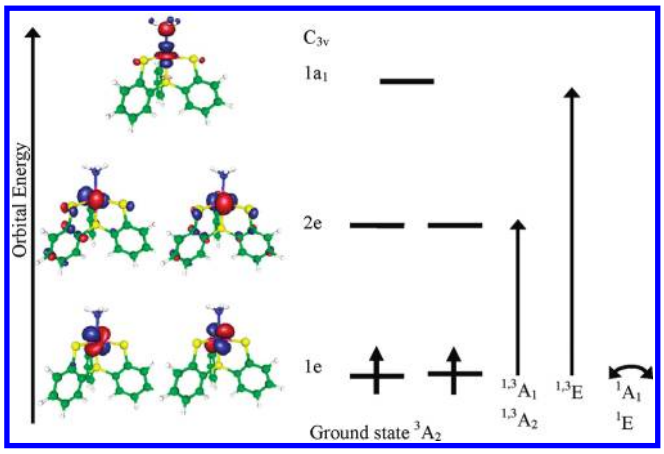

Figure 4. The metal d-based MOs and term symbols arising from single excitations for **4′**. The indicated orbital occupation pattern refers to the $^3A_2$ ground state.

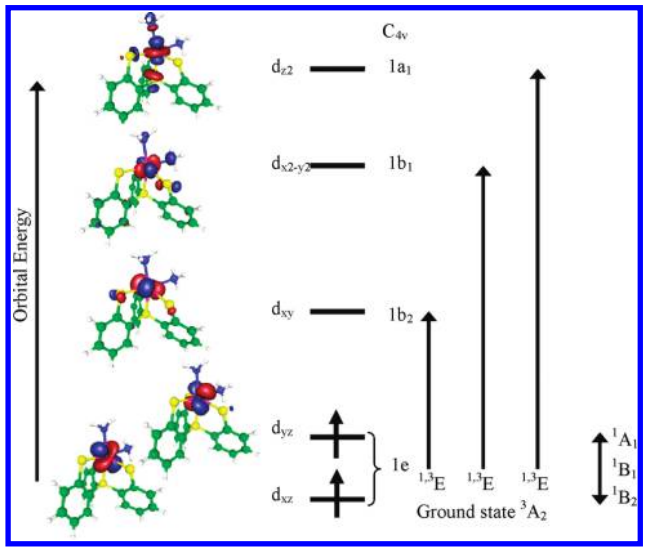

Figure 5. Metal d-based MOs and term symbols (analyzed under approximate C_{4v} symmetry) arising from single excitations for **6′**. The indicated orbital occupation pattern refers to the $^3A_2$ ground state.

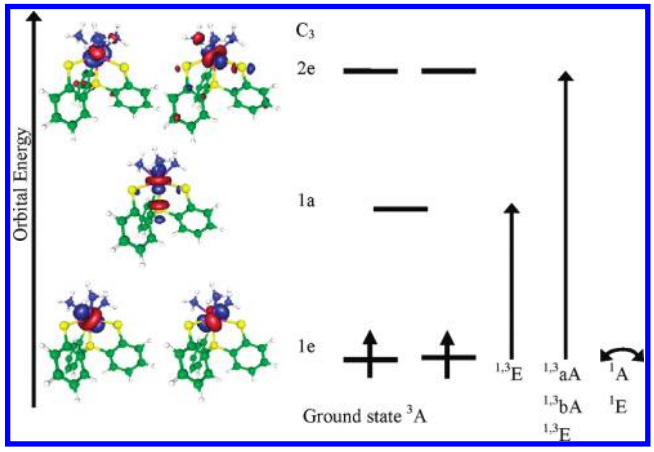

Figure 6. Metal d-based MOs and term symbols arising from single excitations for **7′**. The indicated orbital occupation pattern refers to the ^{3}A ground state.

Using the ligand field type arguments elaborated elsewhere,[69] we obtain:

For **4′**

$$D^{SOC}({}^3A_2) \cong \zeta_V^2 \left[\frac{\alpha^4_{xz,yz}}{\Delta({}^1A_1(1e \rightarrow 1e))} + \frac{1}{2}\frac{\alpha^2_{xz,yz}\gamma^2_{xy,x^2-y^2}}{\Delta({}^3E(1e \rightarrow 2e))} - \frac{1}{2}\frac{\alpha^2_{xz,yz}\gamma^2_{xy,x^2-y^2}}{\Delta({}^1E(1e \rightarrow 2e))} + \frac{3}{4}\frac{\alpha^2_{xz,yz}\beta^2_{z^2}}{\Delta({}^3E(1e \rightarrow 1a_1))} - \frac{3}{4}\frac{\alpha^2_{xz,yz}\beta^2_{z^2}}{\Delta({}^1E(1e \rightarrow 1a_1))} \right] \quad (5)$$

For **6′**

$$D^{SOC}({}^3A_2) \cong \zeta_V^2 \left[\frac{\alpha^4_{xz,yz}}{\Delta({}^1A_1(1e \rightarrow 1e))} + \frac{1}{4}\frac{\alpha^2_{xz,yz}\gamma^2_{xy}}{\Delta({}^3E(1e \rightarrow 1b_2))} - \frac{1}{4}\frac{\alpha^2_{xz,yz}\gamma^2_{xy}}{\Delta({}^1E(1e \rightarrow 1b_2))} + \frac{1}{4}\frac{\alpha^2_{xz,yz}\delta^2_{x^2-y^2}}{\Delta({}^3E(1e \rightarrow 1b_1))} - \frac{1}{4}\frac{\alpha^2_{xz,yz}\delta^2_{x^2-y^2}}{\Delta({}^1E(1e \rightarrow 1b_1))} + \frac{3}{4}\frac{\alpha^2_{xz,yz}\beta^2_{z^2}}{\Delta({}^3E(1e \rightarrow 1a_1))} - \frac{3}{4}\frac{\alpha^2_{xz,yz}\beta^2_{z^2}}{\Delta({}^1E(1e \rightarrow 1a_1))} \right] \quad (6)$$

For **7′** and **7″**

$$D^{SOC}({}^3A) \cong \zeta_V^2 \left[\frac{(2\alpha^2_{xy,x^2-y^2} - \alpha^2_{xz,yz})^2}{\Delta({}^1A(1e \rightarrow 1e))} + \frac{3}{4}\frac{\alpha^2_{xz,yz}\beta^2_{z^2}}{\Delta({}^3E(1e \rightarrow 1a_1))} - \frac{3}{4}\frac{\alpha^2_{xz,yz}\beta^2_{z^2}}{\Delta({}^1E(1e \rightarrow 1a_1))} - \frac{1}{2}\frac{(2\alpha_{xy,x^2-y^2}\gamma_{xy,x^2-y^2} - \alpha_{xz,yz}\gamma_{xz,yz})^2}{\Delta(b^3A(1e \rightarrow 2e))} + \frac{1}{2}\frac{(2\alpha_{xy,x^2-y^2}\gamma_{xy,x^2-y^2} - \alpha_{xz,yz}\gamma_{xz,yz})^2}{\Delta(b^1A(1e \rightarrow 2e))} + \frac{1}{2}\frac{(\alpha_{xy,x^2-y^2}\gamma_{xz,yz} - \alpha_{xz,yz}\gamma_{xy,x^2-y^2})^2}{\Delta({}^3E(1e \rightarrow 2e))} - \frac{1}{2}\frac{(\alpha_{xy,x^2-y^2}\gamma_{xz,yz} - \alpha_{xz,yz}\gamma_{xy,x^2-y^2})^2}{\Delta({}^1E(1e \rightarrow 2e))} \right] \quad (7)$$

Here ζ_V is the one-electron SOC constant for a V(III) 3d electron (~206 cm^{-1}),[70] α_i^2, β_i^2, γ_i^2, and δ_i^2 are the fractional vanadium orbital character of the indicated type ($i = xy$, etc.) in the metal-d based MOs and $\Delta(X)$ is the transition energy from the ground electronic state to the excited state X. A semi-quantitative estimate can be achieved as in Tables 5−8 if we combine the transition energies from the CASSCF (SORCI) calculations with the fractional metal orbital characters from the BP86 calculations.

Inspection of eq 5 and 6 for **4′** and **6′** indicates that there are contributions from several pairs of the excited states $^{3,1}X$. The exception is the positive contribution from intra-SOMO transitions $^1A_1(1e \rightarrow 1e)$ for which there are no triplet counterparts. Each pair yields a positive contribution to the final D value as well. Thus one can qualitatively determine the positive sign of the SOC contribution to the zfs. Quantitatively, the final values of D^{SOC} are in acceptable agreement with those predicted by the CASSCF method (1.9 vs 1.2 cm^{-1} for **4′** and 2.4 vs 2.7 cm^{-1} for **6′**). As shown in Table 5, the

Table 5. Individual Contributions to the D Value (in cm^{-1}) for the Constrained Model **4′** [a]

state	energy (cm^{-1})	contribution to D (cm^{-1})
$\|^1A_1(1e \rightarrow 1e)\rangle$	19560	1.4
$\|^3E(1e \rightarrow 2e)\rangle$	11160	1.0
$\|^1E(1e \rightarrow 2e)\rangle$	20090	0.6
$\|^3E(1e \rightarrow 1a_1)\rangle$	27090	0.6
$\|^1E(1e \rightarrow 1a_1)\rangle$	33820	0.5
total D^{SOC}		1.9

[a] $\alpha^2_{xz,yz} \sim 0.79$, $\gamma^2_{xy,x^2-y^2} \sim 0.69$, $\beta^2_{z^2} \sim 0.66$.

Table 6. Individual Contributions to the D Value for the Constrained Model **6′** [a]

state	energy (cm^{-1})	contribution to D (cm^{-1})
$\|^1A_1(1e \rightarrow 1e)\rangle$	13180	1.6
$\|^3E(1e \rightarrow 1b_2)\rangle$	5460	0.9
$\|^1E(1e \rightarrow 1b_2)\rangle$	17660	0.3
$\|^3E(1e \rightarrow 1b_1)\rangle$	14940	0.2
$\|^1E(1e \rightarrow 1b_1)\rangle$	31390	0.1
$\|^3E(1e \rightarrow 1a_1)\rangle$	28900	0.4
$\|^1E(1e \rightarrow 1a_1)\rangle$	34340	0.3
total D^{SOC}		2.4

[a] $\alpha^2_{xz,yz} \sim 0.71$, $\gamma^2_{xy} \sim 0.68$, $\delta^2_{x^2-y^2} \sim 0.49$, $\beta^2_{z^2} \sim 0.52$.

Table 7. Individual Contributions to the D value for the Constrained Model **7′** [a]

state	energy (cm^{-1})	contribution to D (cm^{-1})
$\|^1A(1e \rightarrow 1e)\rangle$	20850	0.2
$\|^3E(1e \rightarrow 1a_1)\rangle$	15930	0.3
$\|^1E(1e \rightarrow 1a_1)\rangle$	23850	0.2
$\|b^3A(1e \rightarrow 2e)\rangle$	9760	0.2
$\|b^1A(1e \rightarrow 2e)\rangle$	24430	0.1
$\|^3E(1e \rightarrow 2e)\rangle$	23330	0
$\|^1E(1e \rightarrow 2e)\rangle$	27240	0
total D^{SOC}		0.2

[a] $\alpha^2_{x^2-y^2,xy} \sim 0.33$, $\alpha^2_{xz,yz} \sim 0.33$, $\beta^2_{z^2} \sim 0.49$, $\gamma^2_{xy,yz} \sim 0.30$, $\gamma^2_{xy,x^2-y^2} \sim 0.27$.

Table 8. Individual Contributions to the D value for the Constrained Model **7″** [a]

	CASSCF		SORCI	
state	energy (cm^{-1})	contribution to D (cm^{-1})	energy (cm^{-1})	contribution to D (cm^{-1})
$\|^1A(1e \rightarrow 1e)\rangle$	20690	0.3	18000	0.4
$\|^3E(1e \rightarrow 1a_1)\rangle$	14950	0.5	16210	0.4
$\|^1E(1e \rightarrow 1a_1)\rangle$	22900	0.3	22480	0.3
$\|b^3A(1e \rightarrow 2e)\rangle$	10090	0.3	11830	0.3
$\|b^1A(1e \rightarrow 2e)\rangle$	24900	0.1	23300	0.1
$\|^3E(1e \rightarrow 2e)\rangle$	20220	0	20310	0
$\|^1E(1e \rightarrow 2e)\rangle$	27060	0	25200	0
total D^{SOC}		0.3		0.3

[a] $\alpha^2_{x^2-y^2,xy} \sim 0.39$, $\alpha^2_{xz,yz} \sim 0.37$, $\beta^2_{z^2} \sim 0.58$, $\gamma^2_{xz,yz} \sim 0.36$, $\gamma^2_{xy,x^2-y^2} \sim 0.33$.

(69) Neese, F.; Solomon, E. I. In *Magnetoscience − From Molecules to Materials*; Miller, J. S., Drillon, M., Eds.; Wiley: New York, 2003; Vol. IV, pp 345−466.

(70) Bendix, J.; Brorson, M.; Schäffer, C. E. *Inorg. Chem.* **1993**, *32*, 2838–2849.

leading term of the SOC contribution to the zfs in **4′** is the spin-flip intra-SOMO transition $^1A_1$ (1e→1e) with a magnitude exceeding 1 cm^{-1}. In **6′**, this same singlet excited state $^1A_1$ (1e→1e) gives the largest SOC contribution to the **D** tensor. Although the excited state ^3E-(1e→1b$_2$) of the spin-conserving intra-t$_{2g}$ transition has the lowest energy, the small prefactor (1/4) of its contribution strongly reduces its importance relative to the intra-SOMO transitions. In a previous ligand-field analysis on $[V(H_2O)_6]^{3+}$, the contribution from intra-SOMO spin-flip transition was neglected.[71] Without a thorough analysis of the contributions from all excited states, the neglect of spin-flip transitions is physically unreasonable. Especially in the present case the intra-SOMO spin-flip transition gives the leading contribution to the zfs.

In the case of **7′** and **7″**, according to eq 7 the contribution from intra-SOMO spin-flip transitions should be significantly reduced because of the significant mixing of the two e-sets in their SOMOs. In addition the two new terms b^3A(1e→2e) and b^1A(1e→2e) in eq 7 together provide a negative contribution to the final *D* value. Thus one cannot determine the sign of the SOC contribution by simple inspection of eq 7. However, one may expect that the final *D* value should subtly depend on the metal−ligand covalencies of the metal-based d orbitals. Similar to the case of **4′** and **6′**, the semi-quantitative estimates of the D^{SOC} values for **7′** and **7″** agree reasonably well with the CASSCF and SORCI numbers (0.2 vs −0.4 cm^{-1} (CASSCF) for **7′** and 0.3 vs −0.3 cm^{-1} (CASSCF) or 0.1 cm^{-1} (SORCI) for **7″**). As shown in Tables 7 and 8, one cannot identify which excited state gives the leading SOC contribution to the **D** tensor since all contributions have similar magnitudes. It is therefore a challenge to predict the accurate SOC contributions to the final *D* values for these seven coordinate complexes, because one must sum to high precision several contributions of different physical origin but of similar magnitude, yet of varying sign. Comparison of the results from the CASSCF and SORCI calculations in Table 8 reveals that very similar excitation energies were obtained by the two treatments. Using these excitation energies and the fractional vanadium orbital character in the metal d-based MOs from the BP86 calculation, the rather small SOC contributions (∼ 0.3 cm^{-1}) to the zfs were obtained in agreement with the above qualitative considerations. Thus, the leading contribution to the final *D* value in **7′** and **7″** is the direct SSC and *not* the SOC contribution. In this respect CASSCF and SORCI calculations yield different results (vide supra).

Comparison of the absolute magnitude of the SOC contributions to the zfs of the three models shows that **7′** (**7″**) has the smallest SOC of all considered models. In **4′** and **6′**, the intra-SOMO spin-flip transition makes the largest SOC contribution to the **D** tensor, while it is significantly reduced by mixing of the two e-sets ($d_{x^2-y^2,xy}$ vs $d_{xz,yz}$) in **7′** and **7″**. We were curious why this mixing reduces the SOC contribution rather than strengthens it. Under C_3 symmetry the complex d orbitals d_{+2} and d_{-2} have the same transformation properties as d_{-1} and d_{+1}, respectively, and the mixing only can occur between d_{+2} and d_{-1} and between d_{-2} and d_{+1} orbitals. Thus, the mixing of the two e-sets reduces, rather than increases, the orbital angular momentum in each SOMO and hence reduces the SOC between the ground state and intra-SOMO spin-flip excited state via L_z. Inspection of eqs 5−7 reveals that a positive SOC contribution to the final *D* value can be easily deduced in the case of **4′** and **6′**. In **7′** two additional terms from the b^3A(1e→2e) and b^1A(1e→2e) excitations give a net negative contribution to the zfs. This renders determination of the sign of the SOC part by a simple inspection impossible. Under C_{3v} symmetry the two excited states transform as A_2; thus they cannot interact with the A_2 ground state via SOC (in C_{3v} symmetry **L** transforms as A_2 and E). If one neglects any mixing of the SOMOs in **7′** and **7″** by taking $\alpha^2_{x^2-y^2,xy}$ in the 1e-MO and $\gamma^2_{xz,yz}$ in the 2e-MO as zero in eq 7, then eq 7 reduces to eq 5. Therefore the mixing of the two e-sets is the intrinsic reason for the smallest magnitude of the SOC contribution for the seven-coordinate complexes such that the SSC part is the dominant contribution to the **D** tensor.

The significant mixing of the two e-sets in **7′** and **7″** can be ascribed to the geometric feature of the complexes: the large distortion of the V center relative to the plane defined by the three S atoms (0.766 Å in **7** vs 0.216 Å in **4**). A rigid surface scan of the out-of-plane distance of V from the 3S plane toward the 3N plane was carried out with the fixed V-PH_3 bond distance of 2.4 Å. The results (Supporting Information, Figure S3) indicated that the minimum on the calculated potential energy surface occurs at the position of the maximum mixing of the two e-sets. To predict accurate SOC and SSC contributions to the zfs in **7′** or **7″**, it is necessary to calculate the individual contribution of the two-e sets into the SOMOs to high precision. This subtle requirement can apparently not be satisfied by the CASSCF method while the SORCI method can deal with this additional element of complexity.

Discussion

In this work, a detailed combined experimental, quantum chemical, and ligand-field theory analysis of a series of V(III) complexes with PS3 donor ligands has been performed. The first step in the process was the synthesis and structural characterization of the complexes. The series of complexes comprise three coordination numbers, 5 (trigonal bipyramidal: [V(PS3)L]), 6 (distorted octahedral: [V(PS3)(L-L)]), and 7 (monocapped octahedral: [V(PS3)L_3]). These highly variable and non-idealized geometries present a particular challenge to classical methods for analysis of electronic structure, such as crystal-field theory, which are best suited to, for example, octahedral complexes. Moreover, the PS3 ligand differs greatly from the ligand types best described by crystal-field theory, which typically comprise light atom donors (O, N) and are "innocent" in their behavior, for example, complexes of H_2O and NH_3 have no oxidation state ambiguity. The arylthiolate donors of PS3 form highly covalent bonds and can conceivably have thiyl (or even thione) character. Quantum chemical methods, in contrast, make explicit use of the experimental geometries along with optimized geometries

(71) Carver, G.; Spichiger, D.; Tregenna-Piggott, P. L. W. *J. Chem. Phys.* **2005**, *122*, 124511.

and can employ basis sets that explicitly involve all of the atoms present.

To employ these quantum chemical methods, in addition to structural data, it was necessary to characterize the electronic properties of the V(III) ion in each complex using the spin Hamiltonian formalism. Magnetometry confirmed that each complex comprises an $S = 1$ ground state, with essentially the spin-only μ_{eff} at higher temperature. Analysis of the temperature dependent powder susceptibility behavior indicated the presence of zfs. HFEPR, which has been successfully applied to other "EPR-silent" V(III) complexes, yielded accurate and precise values of the spin Hamiltonian parameters for powder samples. In particular, the sign as well as magnitude of the axial zfs parameter, D, was readily determined.

The subsequent quantum chemical analysis allowed deconvolution of the multiple contributing factors to the zfs in these systems. These include both SOC and SSC effects, the latter being often ignored in transition metal complexes. Indeed, the SSC contributions to the **D** tensors are a non-negligible part of the zfs in these vanadium complexes. In the case of the five- and six-coordinate complexes, the direct SSC terms contribute approximately one-third of the final D value. For the seven-coordinate complexes, the SSC contribution exceeds the SOC part and is the largest contribution to the **D** tensor. This is in sharp contrast to the long-followed assumption that in open-shell transition metal complexes the SOC contribution is always the dominant source of the zfs. In fact there is no *a priori* physical justification to neglect SSC contributions in transition metal complexes unless the zfs becomes exceedingly large. Judging from the wealth of experience with organic triplets, one may anticipate that the SSC term may reach up to $1-2\ cm^{-1}$ in magnitude. Hence, only for very large SOC induced D values (i.e., $> 10\ cm^{-1}$) is it justified to neglect this contribution. In other situations the SSC may, or may not, have a significant impact on the zfs. Currently, there does not appear to be enough insight into the variation of the SSC term with molecular structure to make an *a priori* estimate of its importance. Hence more systematic calculations are needed to derive reliable magnetostructural correlations, of which this study represents an early step.

In the particular example here of the seven-coordinate complexes, the reason for the dominance of SSC is as follows. The positive SOC contribution to D from the intra-SOMO spin-flip excitations is significantly reduced by the mixing of the two e-sets ($d_{x^2-y^2,xy}$ vs $d_{xz,yz}$). In addition, owing to the same reason, two new SOC terms arise that in total yield a negative contribution to the final D value. The combination of these two factors results in a minimal SOC contribution and thus the dominance of the SSC contribution.

Concerning the five- and six-coordinate V(III) complexes, for which the SOC part contributes roughly two-thirds of the **D** tensor, it is then desirable to understand these specific contributions. Careful analysis of the individual contribution of each excited state revealed that the spin-flip (i.e, triplet−singlet) terms dominate over the contributions of the spin-conserving excitations (i.e., intra-triplet). Ligand field models that do not take these contributions into account cannot be realistic. The most important spin-flips are the intra-SOMO excitations. If there are very low-lying d-d excited multiplets, one may anticipate that these excited states certainly make the most important contributions to the SOC. But this is not the case for the six-coordinate vanadium complexes. These species possess very low-lying spin-conserving intra-t_{2g} excited states. However, the small prefactor of their contribution significantly decreases their importance to an extent that the intra-SOMO excitation is the leading contribution to the **D** tensor.

Careful analysis indicated that the intra-SOMO spin-flip transitions yield positive contributions to the SOC parts of the **D** tensors for all investigated complexes. If a given excited state ^3X gives a positive contribution to D, we have shown that the corresponding excited state ^1X with the same spatial part but different spin coupling yields a compensating negative contribution and vice versa. Thus, to predict accurate D values for V(III) complexes, it is necessary to calculate small differences among several contributions of similar magnitudes, varying signs, and different physical origins—a challenging task indeed.

Quantitative modeling of the zfs for the all vanadium complexes under investigation requires accurate predictions of the SOC as well as the SSC parts. The value of the SOC term crucially depends on the excitation energies of the most important d-d excited states, especially of the intra-SOMO spin-flip transitions. Second, an accurate SOC part can only be achieved if the metal−ligand bond covalencies are properly described and low-symmetry effects are accurately taken care of. DFT as a single-determinant method is not able to properly describe these spin-flip excited states and thus DFT results significantly underestimate their contributions. In the case of the five- and six-coordinate complexes, the DFT method even predicts the wrong signs of these most important contributions. The CASSCF method, conversely, gives metal−ligand bonds that are too ionic and hence SOC effects will be slightly overestimated. The SORCI method is designed to give accurate transition energies as well as good metal−ligand bond covalencies. It does suffer, however, to some extent from size consistency problems, which means that its predictions potentially deteriorate as the investigated systems become larger. The SORCI method also suffers to some extent from the high computational effort to carry out such calculations for large molecules. Hence, significant further method development is necessary before a fully satisfactory theoretical method is available for transition metal zfs.

An accurate estimation of the anisotropic metal−ligand covalency in the open-shell orbitals is certainly imperative to afford accurate predictions for the SSC part. Especially for **7′** and **7″** this is problematic since there is a very subtle but important mixing of the two e-sets. One has to accurately predict the individual contribution from each e-set to obtain good results for the SSC contribution. In this respect CASSCF has not been successful, while the SORCI method appears to provide good results.

Conclusions

A series of V(III) complexes of varying coordination number (5, 6, and 7) has been prepared and structurally characterized. The complexes all have in common a PS3 ligand, which provides a donor set with relevance to the putative thiolate rich coordination site for V in V-nitrogenase. The complexes are of general formula $[V(PS3)L_n]^{0,-}$, where $n = 1$ (from L = Cl^-, 1-Me-Im, N_3^-), 2 (from L = 2,2′-bpy; counting each N of the bidentate ligand), and 3 (from L = 1-Me-Im, N_2H_4). They have been investigated by

a variety of physical methods, in particular magnetometry and HFEPR. HFEPR has been applied to other V(III) complexes and has been shown to be successful at extracting spin Hamiltonian parameters from this spin triplet that is often difficult to study by EPR at conventional fields and frequencies. HFEPR, supported by magnetometry, has provided accurate zfs values that are then the empirical starting point for computational studies the likes of which have, to our knowledge, been rarely applied to spin multiplet transition metal complexes, and heretofore not to V(III).

DFT methods have shown to be successful in many contexts, however, for the $[V(PS3)L_n]^{0,-}$ complexes studied here (using computational models in which the PS3 ligand type has been simplified) DFT is not very effective in modeling the experimental zfs. More advanced techniques are required. The best results were delivered by SORCI calculations within the quasi-degenerate perturbation formalism.

Certain qualitative conclusions about zfs based on the computational studies should be mentioned, as these are of potentially widespread importance in transition metal complexes. Concerning the SOC contribution to the **D** tensor, the spin-flip singlet excited states give larger contributions than do the spin-conserving triplet excitations, despite the relatively higher energy of the spin singlet excited states relative to spin triplets. This qualitative finding is counter to the common assumption, at least in integer spin (non-Kramers) systems (such as V(III)), which is that zfs is dominated by excited states of the same spin as the ground state. Another common assumption is that the SSC contribution to the **D** tensor is negligible for transition metal complexes. This is not the case for the complexes studied here, which have overall relatively small zfs and the SSC contribution is proportionately large, and indeed the dominant effect in some cases. The overall conclusion, however, is that calculation of zfs for V(III) complexes is a difficult task because the total effect arises from numerous contributions that are often of similar magnitude, but opposite sign. The delicate balance among these effects yields the overall zfs. We hope that the combination of better experimental data, such as those derived from HFEPR,[13,15,20] INS (inelastic neutron scattering),[72] and other techniques,[71] in conjunction with further advances in computational power and methodology will provide a general understanding of spin multiplet transition metal complexes.

Acknowledgment. This work was supported by the National Science Council in Taiwan (NSC 96-2113-M-006-011). S.Y. and F.N. gratefully acknowledge a grant from the German Science Foundation (NE 690/7-1). HFEPR studies were supported by the NHMFL, which is funded by the NSF through Cooperative Agreement DMR 0654118, the State of Florida, and the DOE. The 25 T resistive magnet was funded by the W. M. Keck Foundation. J.T. and J.K. acknowledge NHMFL UCGP grant 5062.

Supporting Information Available: Crystal data and structure refinement for compounds **4**, **6**, and **7** (Table S1); selected bond distances (in Å) and angles (in degrees) for V(III)-thiolate complexes (Table S2); comparison of the calculated metrical parameters (in Å) for the completely optimized models **4′**, **6′**, and **7′** with their corresponding experimental crystal structures **4**, **6**, and **7** (Table S3); magnetic fits for **3**, **6**, and **8** (Figure S1); H-bonding in **8** (Figure S2); evolution of the mixing of the two e-sets in the SOMOs and the total energy for **7″** as a function of the vanadium out-of-plane distance (Figure S3); the syntheses of **4**, **6**, and **7**; the wave functions for the LFT analysis; CIF files for **4**, **6**, and **7**. This material is available free of charge via the Internet at http://pubs.acs.org.

(72) Basler, R.; Tregenna-Piggott, P. L. W.; Andres, H.; Dobe, C.; Güdel, H.-U.; Janssen, S.; McIntyre, G. J. *J. Am. Chem. Soc.* **2001**, *123*, 3377–3378.